Scaling of mixed structure functions in turbulent boundary layers

Boris Jacob, Carlo Massimo Casciola, Alessandro Talamelli, and P. Henrik Alfredsson

Citation: Phys. Fluids **20**, 045101 (2008); doi: 10.1063/1.2898659
View online: http://dx.doi.org/10.1063/1.2898659
View Table of Contents: http://pof.aip.org/resource/1/PHFLE6/v20/i4
Published by the American Institute of Physics.

Scaling of mixed structure functions in turbulent boundary layers

Boris Jacob,[1] Carlo Massimo Casciola,[2] Alessandro Talamelli,[3] and P. Henrik Alfredsson[4]
[1]*INSEAN, via di Vallerano 139, 00128 Roma, Italy*
[2]*Dipartimento di Meccanica e Aeronautica, Università di Roma "La Sapienza," via Eudossiana 18, 00184 Roma, Italy*
[3]*Seconda Facoltà di Ingegneria, Università di Bologna, via Fontanelle 40, 47100 Forlì, Italy*
[4]*Linné Flow Center, KTH Mechanics, Royal Institute of Technology, S-100 44 Stockholm, Sweden*

(Received 10 October 2007; accepted 19 February 2008; published online 1 April 2008)

We address the issue of the scaling of the anisotropic components of the hierarchy of correlation tensors in the logarithmic region of a turbulent boundary layer over a flat plate, at $\mathrm{Re}_\theta \approx 15\,000$. We isolate the anisotropic observables by means of decomposition tools based on the SO(3) symmetry group of rotations. By employing a dataset made of velocity signals detected by two *X* probes, we demonstrate that the behavior of the anisotropic fluctuations throughout the boundary layer may be understood in terms of the superposition of two distinct regimes. The transition is controlled by the magnitude of the mean shear and occurs in correspondence with the shear scale. Below the shear scale, an isotropy-recovering behavior occurs, which is characterized by a set of universal exponents which roughly match dimensional predictions based on Lumley's argument [J. L. Lumley, Phys. Fluids **8**, 1056 (1965)]. Above the shear scale, the competition between energy production and transfer mechanisms gives rise to a completely different scenario with strong alterations of the observed scaling laws. This aspect has significant implications for the correct parametrization of the anisotropy behavior in the near wall region since, approaching the wall, an increasingly larger fraction of the scaling interval tends to conform to the shear-dominated power laws. © *2008 American Institute of Physics*. [DOI: 10.1063/1.2898659]

I. INTRODUCTION

Most turbulent flows encountered in nature or in technological applications are intrinsically anisotropic, which are sustained by mechanisms such as mean velocity gradients, rotation, or stratification. In many circumstances, additional complications are introduced by the presence of physical boundaries. Unfortunately, a solid theory has been developed only under the simplifying assumptions of homogeneity and isotropy.[1] Beyond this situation, description of turbulence statistics is much more limited, even if valuable results have been obtained for specific problems with *ad hoc* assumptions. Yet, improving the characterization of the anisotropy effects on the flow structure is not only of great theoretical importance, but is also a key ingredient for the development of reliable tools for flow prediction.[2]

As well known, most popular numerical methods, either large eddy simulations or Reynolds averaged Navier–Stokes (RANS) equations, do not perform well in many cases of practical importance, in particular, when the mean deformation rate is comparable or larger than the inverse turbulent time scale. The basic reason behind this failure has to do with a poor characterization of the velocity field anisotropy, which is usually done only in terms of few global indicators. In many models, anisotropy effects are simply neglected by relying on Kolmogorov phenomenology in which turbulent fluctuations become isotropic at the small scales of high Reynolds number flows, regardless of the detail of forcing and boundary conditions.[1] This picture, which is considered a good working approximation until recently, is getting progressively refined. Actually, the possibility of persistence of anisotropy in the small scales was clearly recognized in a few papers in the 1990s.[3,4] More recently, numerical and experimental works[5–7] confirm that anisotropy may persist in shear flows even at very high Reynolds numbers. In any case, in the presence of strong anisotropy, the very basic premise to Kolmogorov theory is questionable, i.e., no sufficiently large number of cascading steps may exist through which the forcing-dependent properties are progressively smeared out. In these conditions, important departures from Kolmogorov predictions are expected over the entire range of scales.

The most appropriate tool to discuss departure from isotropy is based on a general decomposition of tensor fields in terms of certain basis functions able to probe increasingly complex levels of anisotropy, the so-called SO(3) decomposition (see Ref. 8 for a comprehensive review of the subject in the context of turbulence). For a scalar, this approach reduces to a standard expansion in spherical harmonics where the basis functions are hierarchically organized in sectors progressively numbered $j=0,1,\ldots$ (see, e.g., the ordering of orbitals in the hydrogen atom). Each sector j is a subspace spanned by $2j+1$ spherical harmonics Y_{jm}, which is invariant under rotations and is characterized by a certain type of anisotropy. The extension of these concepts to tensor fields has proved useful in the past decade to rationalize the issue of small scale isotropy recovery in turbulent flows.[9–18] The major conclusion of these investigations is that, under weak anisotropy, a universal route to isotropy recovery exists, with the isotropic component of the velocity field always providing the leading contribution to the expansion at small scales.

Our purpose here is to investigate how a strong shear alters this nowadays well established pattern to understand how anisotropy may persist in the small scales of high Reynolds number shear flows. This issue has been addressed numerically in a recent paper by means of direct numerical simulations of the homeogeneous shear flow.[19] In the present paper, we use, instead, an experimental approach similar to that described in Ref. 18. We focus, in particular, on the leading anisotropic component of the statistics of the velocity field, which is isolated by means of particular multipoint observables selected with the help of the SO(3) decomposition. A discussion of the behavior of the isotropic sector under strong shear may be found in Ref. 20. We use the Minimum Turbulence Level (MTL) wind tunnel at KTH which gives well controlled conditions at a high Reynolds number (in this case $\mathrm{Re}_\theta = 15\,000$), allowing us to overcome usual resolution limitations. In such a way, we are able to characterize the scale-dependent anisotropic features of turbulence throughout the entire logarithmic region of the boundary layer.

II. ANGULAR DEPENDENCE OF CORRELATION TENSORS

As anticipated, the SO(3) decomposition is used to extract the anisotropic components from the complete velocity field. For our purposes, it is sufficient to recall here that the technique allows one to distinguish among different kinds of anisotropies by projecting generic statistical quantities, e.g., correlation tensors, on a suitable basis formed by the eigenfunctions of the infinitesimal generator of the rotation group SO(3). The method has been described in great detail in several papers, see, e.g., Refs. 8–10, and has been successfully implemented both in numerical works (random Kolmogorov flow[13] and channel flows at small Reynolds numbers[14]) and experimental investigations (atmospheric boundary layer,[9–12] homogeneous shear flows,[16–18] flat plate boundary layer[18]).

By first denoting the velocity difference component between two points separated by $\mathbf{r}$ as $\delta v_{\alpha_1}(\mathbf{r})$, where $\alpha_1 = 1$, 2, or 3, we can define the velocity structure tensor of order 2 as $S_{\alpha_1\alpha_2}(\mathbf{r}) = \langle \delta v_{\alpha_1}(\mathbf{r}) \delta v_{\alpha_2}(\mathbf{r}) \rangle$. The decomposition for $S_{\alpha_1\alpha_2}(\mathbf{r})$ then reads

$$S_{\alpha_1\alpha_2}(\mathbf{r}) = \sum_{j=0}^{\infty} \sum_{m=-j}^{+j} \sum_{q=1}^{p(j)} S^{(2)}_{jmq}(r) B^{jmq}_{\alpha_1\alpha_2}(\hat{\mathbf{r}}). \tag{1}$$

Here, the index j denotes a *sector* of the SO(3) decomposition, i.e., a subspace of dimension $2j+1$ invariant under rotations. Eigenfunctions pertaining to sector $j=0$ are constant under the solid angle, thus accounting for the isotropic part of the object. Higher j's contain increasing degrees of anisotropy. The tensorial nature is described by the indices α_1, α_2 of the basis elements $B^{jmq}_{\alpha_1\alpha_2}(\hat{\mathbf{r}})$, where the unit vector $\hat{\mathbf{r}} = \mathbf{r}/r$ provides the dependence on the two angles, azimuthal and polar, say, which parametrize the unit sphere. Here, m ranging from $-j$ to j denotes one of the independent elements of the functional basis, i.e., the spherical harmonics, in sector j. Without entering here in more detail, we like to provide the unfamiliar reader with a feeling concerning the need for index q. In the functional expansion for a scalar field, i.e., in the standard spherical harmonics, the index q does not appear at all. This corresponds to the fact that a scalar is a tensor of order zero. When moving from scalars to vector and tensor fields of increasing order, the space dependence is still captured by the spherical harmonics being functions of the angles $\hat{\mathbf{r}}$ and the indices j, m and by the r dependence of the coefficients $S^{(2)}_{jmq}$. In addition, to take care of the local algebraic base for tensors, a certain number of independent elements is necessary, e.g., in principle, 3 for vectors or 9 for second order tensors. This fact is accounted for by the basis elements $B^{jmq}_{\alpha_1\alpha_2}$ with $q = 1, \ldots, p(j)$ for given j, m, where α_1 and α_2 specify, e.g., the Cartesian components. Clearly, for second order tensors, $p(j) \leqslant 9$, which is less than the maximum only if the symmetry of the sector reduces the number of independent elements allowed. This happens, e.g., in the isotropic sector $j=0$. Actually, as well known, the most general isotropic second order tensor field is expressed as $A(r)\delta_{\alpha\beta} + B(r) r_\alpha r_\beta + C(r)\epsilon_{\alpha\beta\gamma} r_\gamma$, implying that $p(0)=3$. The coefficients $S^{(2)}_{jmq}(r)$ of the expansion carry the information concerning the scaling behavior of the observable.

Expansion (1) for the second order correlation tensor can be generalized to correlation tensors $S_{\alpha_1 \cdots \alpha_n}(\mathbf{r}) = \langle \delta v_{\alpha_1}(\mathbf{r}) \cdots \delta v_{\alpha_n}(\mathbf{r}) \rangle$ of order n and their components $S^{(n)}_{jmq}(r)$ represent the key objects of the theory.

In the case of *weak* anisotropy, experimental and numerical evidences[8] support the conjecture that different projections in the same sector j display the same power-law behavior, with a scaling exponent $\zeta_j(n)$ independent of m and q. Order of magnitude estimates for such exponents are provided by dimensional analysis, $\zeta_j(n) = (j+n)/3$,[15] by generalizing an argument first put forward by Lumley for the cospectrum.[21] In fact, the actual exponents may substantially differ from dimensional predictions—the so-called intermittency correction—unless the order of the structure function n and of the sector j are sufficiently low. Clearly, the problem cannot be attacked on the purely theoretical ground starting from the Navier–Stokes equations. At any rate, the available experimental and numerical data display a hierarchical organization of the scaling exponents, whereby the anisotropic power laws decay faster than the isotropic component $[\zeta_0(n) < \zeta_j(n)]$, so that, in the limit of large Reynolds numbers, the isotropic part makes up the leading term of the decomposition at sufficiently small scales. In this sense, isotropy is recovered at small separations, as concluded in a number of recent numerical and experimental investigations (see again Ref. 8) for a review.

We will show in the following how a strong shear modifies this conclusion to explain the conditions under which the anisotropy may persist down to the viscous scales and affect the gradient statistics.

III. ANISOTROPY EXTRACTION

A precise assessment of the exponents $\zeta_j(n)$ is hampered by many obstacles. In numerical applications, the projections on the different sectors can be straightforwardly performed. However, ambiguities associated with the modest extent of inertial ranges typical of current direct numerical simulations arise. On the experimental side, on the contrary, only the

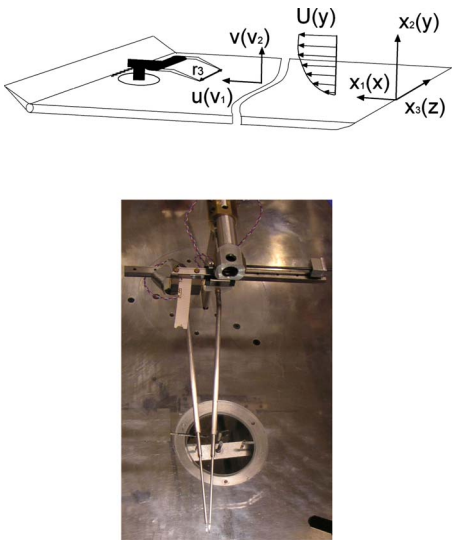

FIG. 1. (Color online) Top: Sketch of the experimental setup together with the coordinate system. Bottom: Picture of the probe setup, showing the two inclined supports for the X wires and the spanwise traversing mechanism. For reference, the circular Plexiglas plug has a diameter of 50 mm.

scaling of some sectors is accessible by probing the behavior of particular components of correlation tensors in suitable directions so as to cancel out the contribution from the isotropic part. For instance, at second order, quantities such as $S_{12}(r_1)$ or $S_{12}(r_3)$ turn out to be dominated by the projection on sector $j=2$, enabling the measurement of $\zeta_2(2)$ (see, e.g., Ref. 9 or 16). Similarly, measurements in sector $j=1$ have been performed in the atmospheric boundary layer by addressing the behavior of antisymmetric quantities evaluated from temporal data gathered by fixed probes.[10] More complicated experimental configurations are needed in order to directly probe spatial dependence, as done in, e.g., Ref. 18. There, the exponent in sector $j=2$ has been directly measured for homogeneous shear turbulence, and the extracted value was found appropriate to reproduce the statistics in the outer part of the logarithmic region of turbulent boundary layers. However, closer to the wall, the quality of the prediction degraded. An explanation for this discrepancy, as well as new features of anisotropy fluctuations, will be provided here based on new measurements performed in a larger facility at higher Reynolds numbers.

IV. EXPERIMENTAL SETUP

The measurements were made in the MTL wind tunnel at KTH using the standard flat plate setup described by Österlund[22] (see also Ref. 23 for a recent experiment). The instrumentation setup consists of two X-wire probes oriented so as to measure the instantaneous velocity components ($u=v_1$ and $v=v_2$) in the streamwise ($x=x_1$) and wall-normal ($y=x_2$) directions. Both probes are positioned with a common traversing system at the same height from the plate and can be moved apart in the spanwise direction (x_3) with separation r_3 ranging approximately from 1 up to 60 mm by means of a second traversing system (see Fig. 1). Both the active length and the separation between wires of the probes are 0.5 mm with a wire diameter of 2.5 μm. The wires were connected to an AN1003 anemometer system and run at an overheat ratio of 1.7. They were calibrated in the free stream versus the angle by means of a pitching device (by first rotating them by 90°).

Data were acquired at approximately 5.45 m from the leading edge of the plate and at a free stream velocity of 26.6 m/s. The integral parameters of the boundary layer at the measurement position are summarized in Table I. In the present work, the friction velocity u_τ was determined from a Clauser plot and gave a value in good agreement with previous oil film measurements (see also Ref. 22 for a detailed characterization of the flow).

A good compromise between the conflicting issues of spatial resolution and Reynolds number requirements is obtained by restricting the measurements to the logarithmic region, in the range $y^+ \approx 100-750$. In Table II, we give the relevant parameters at the two representative positions where most of the discussion will be focused.

We accumulated sufficient statistics ($\sim 5\times 10^6$ samples) to be confident on the anisotropic quantities up to order 6, e.g., $S_{111112}(r_3)$ and similar quantities listed in Table III. Since the prerogative of this setup is its ability to directly measure spatial correlations in the transverse direction without resorting to additional assumptions, the main concern of the paper will be on such objects. In any case, we have also examined the scaling of traditional single-probe anisotropic quantities computed with the help of Taylor hypothesis, such as $S_{12}(r_1)$ (Ref. 16) or the shear-stress cospectrum $E_{12}(k_1)$.[24] In our conditions, however, the longitudinal structure functions did not show any well-defined scaling and will not be further discussed here.

V. EXPERIMENTAL RESULTS

An overall impression of the impact of anisotropy on turbulent statistics as the wall is approached is provided in Fig. 2. Here, the mixed structure function of order 2, $S_{12}(r_3)$, is computed as a function of spanwise separation at different wall-normal distances, ranging from $y^+=750$ down to $y^+=60$. Although for the measurement points closest to the wall resolution issues may arise, they do not flaw the qualitative picture. For quantitative purposes, we focus only on the region above $y^+=180$ in the following.

TABLE I. Integral parameters of the zero pressure gradient boundary layer.

U_∞ (m s^{-1})	x (m)	θ (mm)	δ (mm)	Re_θ	u_τ (m s^{-1})
26.6	5.50	8.1	55	15 000	0.91

TABLE II. Basic turbulent quantities at two representative measurement locations in the boundary layer. Here, L is the transverse integral scale obtained from the zero crossing in the spanwise correlation of the streamwise velocity component, η is the Kolmogorov length scale, and Re_λ is the Reynolds number based on the Taylor microscale. For the last two quantities, the averaged dissipation rate is needed and was obtained by integrating the dissipation spectra of the streamwise velocity (assuming isotropy).

y^+	u_{rms} (m s^{-1})	v_{rms} (m s^{-1})	ρ_{uv}	L (mm)	η (mm)	Re_λ
750	1.88	0.92	−0.41	18	0.12	750
…	…	…	…	…	…	
180	2.05	0.85	−0.38	13.5	0.09	680

The quantity $-S_{12}(r_3)/[S_{11}(r_3)\cdot S_{22}(r_3)]^{1/2}$, which is normally used to assess the scale dependence of the velocity-difference anisotropy, is shown in the inset of Fig. 2. This quantity should be zero at isotropic scales while approaching $-\overline{uv}/u_{\mathrm{rms}}v_{\mathrm{rms}}\approx 0.4$ for large separations in the logarithmic region.

In the outer part of the logarithmic region, the scaling exponent fitted from the data, $\zeta_2(2)=1.22\pm 0.03$, matches those found when deviations from the isotropic state are small, i.e., under weak shear. In these conditions, a typical value taken from the literature[8] for $\zeta_2(2)$ is 1.22, which, since both n and j are small, is not too far from the dimensional prediction by Lumley,[21] $\zeta_2(2)=\frac{4}{3}$. The comparison of $\zeta_2(2)$ with the corresponding exponent in the isotropic sector under weak shear, $\zeta_0(2)\simeq 0.7\simeq\frac{2}{3}$, shows that isotropy is eventually recovered at small separations in the high Reynolds number limit. Actually, the anisotropic component of the structure function, $S^{(A)}_{\alpha\beta}$, decays like $r^{\zeta_2(2)}$ much faster than the corresponding isotropic part $S^{(I)}_{\alpha\beta}\propto r^{\zeta_0(2)}$, which eventually dominates the small scale range. This is fully consistent with the conclusions drawn in Ref. 24 on the basis of second order statistics gathered in rough-wall turbulent boundary layers.

On the contrary, closer to the wall, recovery of isotropy appears to progress at a much lower rate, as shown by the slower approach toward zero of the anisotropy indicator in the inset of Fig. 2. Quite understandingly, the influence of the imposed mean shear is exerted on the entire spectrum of scales. An additional factor preventing the eventual return to isotropy is the decrease of the integral spanwise length scale in this region (due to the effect of the wall), which erodes the extent of the small scale interval.

To address the issue in more detail, we now consider two extreme situations, the upper bound of the logarithmic layer, $y^+=750$, and the lower part of the same region, $y^+=180$. The corresponding anisotropic structure functions of order 6, $S_{111112}(r_3)$, are plotted in Figs. 3 and 4, respectively. At $y^+=750$, a neat scaling over almost one decade above the Kolmogorov scale appears. Given the symmetry of the observable, projections on odd-indexed sectors vanish, and sector $j=2$ provides the leading contribution. By assuming the hierarchical ordering for the exponents, contributions from $j=4$ onward are subleading, and the mixed structure function follows a power law in the form $S_{111112}(r_3)\sim r_3^{\zeta_2(6)}$. At this location, the quality of the scaling allows the exponent to be safely extracted by a direct fit of the data versus scale separation, yielding a figure of $\zeta_2(6)=2.43\pm 0.15$. Similarly, anisotropic moments of lower order ($n=2,4$) also obey power laws with well-defined exponents (see Table IV). Their agreement with the values measured in other conditions, namely, a homogeneous shear flow at similar shear rate parameter,[18] is remarkable, see also the inset of Fig. 3 for a direct comparison of the fourth order anisotropic moment measured in both configurations. All the values we measure in the high logarithmic region are consistent with those found by other authors for weak shear flows, as reported in Ref. 8 where different data sets systematically yield values

TABLE III. The purely anisotropic quantities of different order n on which the present paper will focus (see also Fig. 1 in the following for the definition of the coordinate system employed). Each of these observables is dominated by the contribution of sector $j=2$, thus obeying power laws in the form $r^{\zeta_2(n)}$.

$n=2$	$-S_{12}(r_3)$		
$n=4$	$-S_{1112}(r_3)$	$-S_{1222}(r_3)$	
$n=6$	$-S_{111112}(r_3)$	$-S_{111222}(r_3)$	$-S_{1222222}(r_3)$

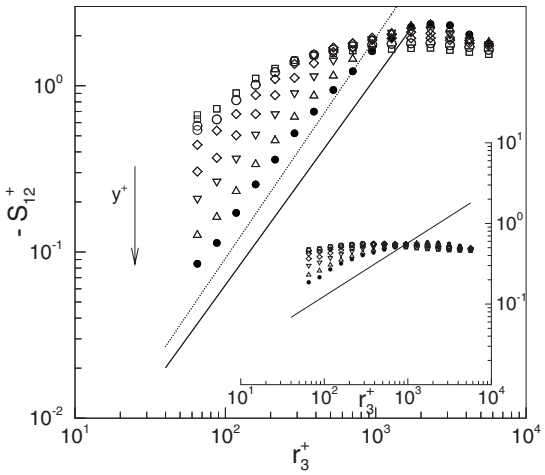

FIG. 2. Main panel: Distribution of the mixed structure function of order 2, $S_{12}(r_3)$ across the logarithmic region. From top to bottom, symbols correspond to locations from $y^+=60$ up to $y^+=750$. The dotted line corresponds to Lumley's dimensional prediction (Ref. 21), $-S_{12}\sim r_3^{1.33}$, while the solid line represents the best fit of the data at $y^+=750$, $-S_{12}\sim r_3^{1.22}$. Here, as in the following, the separation r_3 is made dimensionless with the viscous scale $\ell^*=\nu/u_\tau$, while proper powers of u_τ are used for structure functions. Inset: The anisotropic indicator given by the ratio $-S_{12}/(S_{11}\cdot S_{22})^{1/2}$ (symbols as in the main panel). The solid line represents the decay expected on dimensional grounds with exponent 0.66.

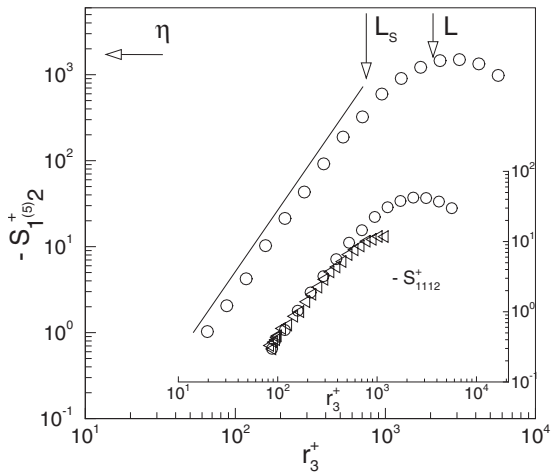

FIG. 3. Main panel: The mixed structure function of order 6, S_{111112} as function of the transverse separation r_3 measured at the outer edge of the logarithmic layer, $y^+=750$ (○). The solid line represents the best fit of the data in the scaling region, $-S_{111112}\sim r_3^{2.43}$. The Kolmogorov scale η, the shear scale $L_S=\kappa y$, and the integral scale L are indicated by arrows. Inset: The most energetic mixed structure function of order 4, S_{1112}, at $y^+=750$ in the boundary layer (○) is compared to that measured in the homogeneous shear flow of Ref. 18 (◁).

for $\zeta_2(6)$ in the range 20–2.3 [for $n=4$, one has $\zeta_2(4)=1.8\pm0.15$].

At vanishing shear, therefore, a *unique* set of scaling exponents is sufficient to provide the leading anisotropic correction to Kolmogorov description of the inertial range. At finite shear, however, such a correction is appropriate only for the isotropy-recovering range, which is well below the scales of energy injection. The upper bound of the isotropy-recovering range can be determined on the basis of a scale energy budget and is controlled by the *shear scale* $L_S=\sqrt{(\epsilon/S^3)}$, for more details see Ref. 25. In the logarithmic layer, where energy dissipation and production balance, assuming $-\overline{uv}=u_\tau^2$, the shear scale is proportional to the wall-

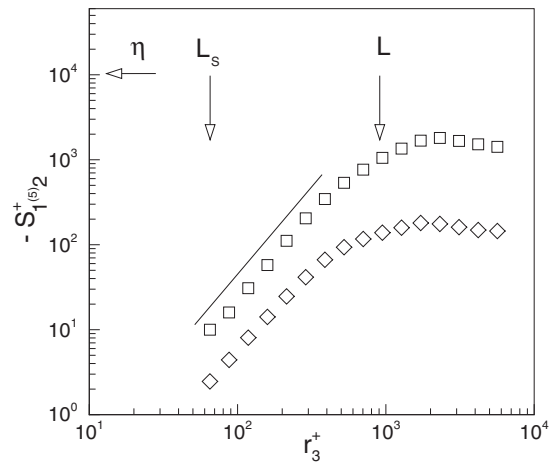

FIG. 4. Mixed structure functions of order 6 measured in the lower part of the logarithmic layer at $y^+=180$ [S_{111112} (□) and S_{111222} (◇)]. The solid line represents the best fit of the data in the scaling region, $S_{111112}\sim r_3^{2.05}$. The scaling exponent for S_{111222} is found to be $\zeta_2(6)=1.87$. The arrows indicate the positions of Kolmogorov scale η, shear scale $L_S=\kappa y$, and integral scale L.

TABLE IV. Exponents $\zeta_2(n)$ of the anisotropic structure functions of different orders, $n=2-6$, as measured by a direct fit vs spanwise separation r_3 at $y^+=750$.

$n=2$	$-S_{12}(r_3)$		
	1.22 ± 0.03		
$n=4$	$-S_{1112}(r_3)$	$-S_{1222}(r_3)$	
	1.89 ± 0.05	1.72 ± 0.05	
$n=6$	$-S_{111112}(r_3)$	$-S_{111222}(r_3)$	$-S_{1222222}(r_3)$
	2.43 ± 0.15	2.28 ± 0.15	2.05 ± 0.15

normal distance and one obtains $L_S=\kappa y$, where $\kappa\approx0.4$ is the Kármán constant. At our uppermost position, $y^+=750$, a wide range of separations r_3 do, indeed, satisfy the condition $r_3<L_S$ (see Fig. 3) and allows the isotropy-recovering scaling to be clearly detected.

Closer to the wall at $y^+=180$, the situation is different, as illustrated in Fig. 4 showing the behavior of two different mixed structure functions of order 6. At this wall-normal position, the shear scale $L_S\sim\kappa y$ is approximately 1.3 mm, roughly corresponding to our smallest resolved scale. Thus, it turns out that we are now probing only the interval of scales governed by the energy injection process, namely, the separations $L_S<r_3<L$.

At $y^+=180$, the most remarkable feature is the well-defined scaling that occurs despite the strong anisotropy. Yet, the exponents differ quite substantially from those evaluated at $y^+=750$. Actually, direct fits for the most energetic moments at orders 2, 4, and 6 yield $\zeta_2(2)=0.97\pm0.04$, $\zeta_2(4)=1.55\pm0.07$, and $\zeta_2(6)=2.05\pm0.15$, see Table V. It is a recurrent feature that the exponents slightly depend on the specific combination of indices appearing in the considered structure function, i.e., u_2-dominated structure functions manifest a slightly lower scaling exponent than the u_1-dominated ones. Even accounting for this spreading, the range of exponents found in the shear dominated regime is well separated from that found in the isotropy-recovering regime. Moreover, since the difference with the universal isotropy-recovering exponents is much larger than typical intermittency corrections, the new values found above L_S must be understood as the distinctive signatures of the shear.

By combining the previous findings, a crossover between two distinct *regimes* is expected, at any given wall-normal distance, at a scale $\mathcal{O}(L_S)$ controlled by the magnitude of the local mean shear. As an example, the two curves

TABLE V. Exponents $\zeta_2(n)$ of the anisotropic structure functions of different orders, $n=2-6$, as measured by a direct fit vs spanwise separation r_3 at $y^+=180$.

$n=2$	$-S_{12}(r_3)$		
	0.97 ± 0.04		
$n=4$	$-S_{1112}(r_3)$	$-S_{1222}(r_3)$	
	1.55 ± 0.07	1.36 ± 0.07	
$n=6$	$-S_{111112}(r_3)$	$-S_{111222}(r_3)$	$-S_{1222222}(r_3)$
	2.05 ± 0.15	1.87 ± 0.15	1.67 ± 0.15

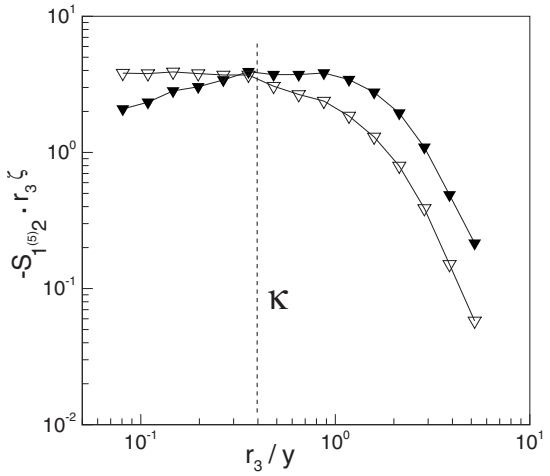

FIG. 5. The mixed structure function of order 6, $S_{111112}(r_3)$ at $y^+=430$, compensated with the exponent of the isotropy-recovering regime $\zeta_2(6)=2.43$ (▽) and with the exponent of the shear-dominated regime, $\zeta_2(6)=2.05$ (▼). Two plateaus, below and above the shear scale, are apparent.

in Fig. 5, relative to $y^+=430$, correspond to the same mixed structure function of order 6 premultiplied first with $r^{\zeta_2(6)}$, as obtained at $y^+=180$ $[\zeta_2(6)=2.43]$ and then with $r^{\zeta_2(6)}$ where the exponent is now taken at $y^+=750$ $[\zeta_2(6)=2.05]$. The two nearby plateaus, each spanning a fairly large interval (almost half a decade wide), clearly show the two subranges sharply separated by the local shear scale $L_S \sim y$.

To further illustrate this result, the collection of the data from all measurement points between $y^+=60$ and $y^+=750$ are plotted in Fig. 6 in the same way as in Fig. 5 and arbitrarily shifted in the vertical direction to fall on top of each other. The normalization of r_3 with y allows to collapse the crossover at a common point for all the curves $(L_S/y=k)$. Quite evidently, a combination of the two fundamental scalings is

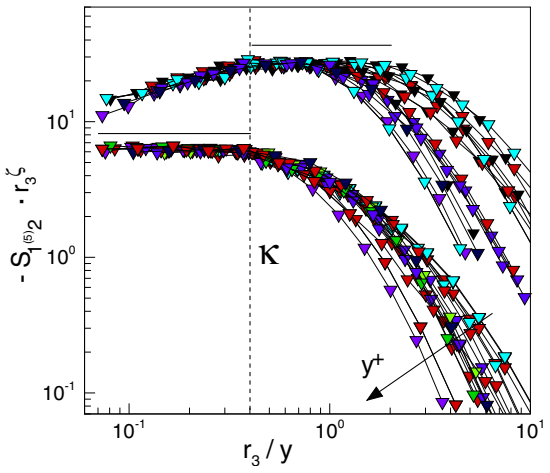

FIG. 6. (Color online) As in Fig. 5, the mixed structure function of order 6, $S_{111112}(r_3)$, at different wall-normal distances $y^+=100-750$ is compensated with the two scaling exponents, pertaining to the isotropy-recovering and shear-dominated regimes, respectively. In both cases, data are arbitrarily shifted to have the curves falling one on top of the other. For the lower group of curves, the isotropy-recovering scaling exponent $\zeta_2(6)=2.43$ is measured by direct fitting at $y^+=750$. For the upper group, the shear-dominated value $\zeta_2(6)=2.05$ is inferred from measurements at $y^+=180$.

able to reproduce the mixed structure function across the full logarithmic region in the entire range of scales below L and above η.

VI. IMPLICATIONS FOR SMALL SCALE ANISOTROPY

The present findings have particular relevance for the persistence of anisotropy in the velocity gradients of the near-wall region. Just to fix ideas, let us consider the pseudo-dissipation tensor

$$\epsilon_{\alpha\beta} = 2\nu \left\langle \frac{\partial u_\alpha}{\partial x_\gamma} \frac{\partial u_\beta}{\partial x_\gamma} \right\rangle,$$

which is a quantity of particular relevance in certain RANS models based on Reynolds stress transport.[2] Clearly, $\epsilon_{\alpha\beta}$ stems from the small scale limit of the second order structure tensor $S_{\alpha\beta}$, $\epsilon_{\alpha\beta} \propto S_{\alpha\beta}/\eta^2$, where $\eta=(\nu^3/\epsilon)^{1/4}$ is the Kolmogorov scale. The anisotropic component of $\epsilon_{\alpha\beta}$, hereafter denoted by $\epsilon^{(A)}_{\alpha\beta}$, is then related to the anisotropic part of $S_{\alpha\beta}$, which is denoted as before by $S^{(A)}_{\alpha\beta}$. As previously shown, $S^{(A)}_{\alpha\beta}$ is dominated by its projection on sector $j=2$. Subdividing[19] the inertial interval into the shear-dominated range above L_S $(L_S \ll r \ll L)$ and isotropy recovery range below L_S $(\eta \ll r \ll L_S)$, the scaling behaviors for $S^{(A)}_{\alpha\beta}$ in the two subranges are $S^{(A)}_{\alpha\beta} \propto r^{\zeta^S_2(2)}$ and $S^{(A)}_{\alpha\beta} \propto r^{\zeta^I_2(2)}$, respectively, with $\zeta^S_2(2) < \zeta^I_2(2)$ as the corresponding scaling exponents (see Tables IV and V). We then obtain the estimate for the anisotropic component of the second order structure tensor at scale η as

$$S^{(A)}_{\alpha\beta}(\eta) \simeq S^{(A)}_{\alpha\beta}(L) \left(\frac{L_S}{L}\right)^{\zeta^S_2(2)} \left(\frac{\eta}{L_S}\right)^{\zeta^I_2(2)}.$$

Since at large scales $S^{(A)}_{\alpha\beta}(L) = \langle \delta u_\alpha(L)\, \delta u_\beta(L) \rangle \propto \langle u_\alpha u_\beta \rangle^{(A)}$, where the latter quantity is the anisotropic contribution to the velocity correlation, we end up with

$$\epsilon^{(A)}_{\alpha\beta} \propto \frac{S^{(A)}_{\alpha\beta}(\eta)}{\eta^2} = \frac{\langle u_\alpha u_\beta \rangle^{(A)}}{\eta^2} \left(\frac{L_S}{L}\right)^{\zeta^S_2(2)} \left(\frac{\eta}{L_S}\right)^{\zeta^I_2(2)},$$

which expresses the amount of anisotropy expected in the gradient given the anisotropy at large scales and the relative position of integral, shear, and Kolmogorov scales. Traditionally, a shear flow is parametrized in terms of two dimensionless quantities, the shear strength $S_* = Su^2/\epsilon = (L/L_S)^{2/3}$, and Corrsin parameter $S_c = \sqrt{S^2\nu/\epsilon} = (\eta/L_S)^{2/3}$. In these terms, we find

$$\epsilon^{(A)}_{\alpha\beta} \propto \frac{\langle u_\alpha u_\beta \rangle^{(A)}}{\eta^2} \frac{S_c^{(2/3)\zeta^I_2(2)}}{S_*^{(2/3)\zeta^A_2(2)}}.$$

We observe that, in the logarithmic layer, $L_S \propto y$, while $\eta \propto y^{3/4}$, hence approaching the wall $\eta/L_S = \mathcal{O}(1)$. In these limiting conditions, the anisotropy in the second order statistics of the gradients is thus completely controlled by the shear-dominated exponents $\zeta^S_2(2)$, i.e., $\epsilon^{(A)}_{\alpha\beta} \propto S_*^{-(2/3)\zeta^A_2(2)}$ or $\epsilon^{(A)}_{12} \propto \langle uv \rangle S_*^{-0.65}/\eta^2$.

VII. SUMMARY

We have experimentally analyzed the scaling behavior of the anisotropic component of the velocity field throughout the logarithmic region of a turbulent boundary layer over a flat plate. The observables used in this study are particular components of the correlation tensor with null projection on the isotropic sector. As customary with experimental data, the extraction of the exponents relies on their relative ordering, in such a way that a purely anisotropic observable is dominated by the sector with smallest j, in our case $j=2$. In principle, the estimate is thus contaminated by subleading contributions from all the other sectors with nonvanishing projection. Clearly, the hierarchical ordering of the exponents cannot be proved in this way and calls for more complete data, which are typically of numerical origin. The issue already settled for the universal isotropy-recovering range[8] has been assessed recently for strong shear flows through numerical simulations of the homogeneous shear flow.[19] Our results here show that, at any particular distance from the wall, the full information concerning anisotropy fluctuations can be efficiently parametrized in terms of two distinct sets of scaling exponents, each pertaining to a well-identified interval of scales. The demarcation between the two subranges is provided by the shear scale L_S, which reflects the intensity of the mean shear. In the logarithmic layer, this quantity is proportional to the distance from the wall. In the interval of scales below L_S, the universal isotropy-recovering dynamics takes place, which is characterized in terms of universal scaling parameters, i.e., scaling exponents common to all situations where the mean shear is only a first order perturbation. Turbulent scales above the shear scale are on the contrary strongly affected by the presence of the mean velocity gradient. In this interval of separations, the anisotropic fluctuations continue to exhibit power laws, yet with substantially lower exponents (see also Ref. 19). This behavior can provide an explanation for the persistent anisotropy found in the small scales of certain shear flows.[16] In the near wall region, where the classical isotropy recovery range below the shear scale shrinks to zero approaching the wall, the scaling exponents in the shear-dominated range allows us to estimate the amount of residual anisotropy to be expected in the dissipative range, hence in the gradient statistics. It is important to note that the differences in the two scaling behaviors, below and above the shear scale, are evident already in second order statistics. This makes the present findings potentially interesting in view of attempts to introduce anisotropic refinements into turbulence models.

ACKNOWLEDGMENTS

We thank the Swedish Foundation for International Cooperation in Research and Higher Education (STINT) for a grant for cooperation between KTH and the University of Bologna. The work of C.M.C. and B.J. has been partially supported by MURST through PRIN05. Support to B.J. was also provided by INSEAN through Programma Ricerche INSEAN July 2006–December 2007 granted by the Italian Ministry of Transportations.

[1] A. N. Kolmogorov, "The local structure of turbulence in an incompressible fluid for very large Reynolds numbers," Dokl. Akad. Nauk SSSR **30**, 299 (1941) [reprinted in Proc. R. Soc. London, Ser. A **434**, 9 (1991)].
[2] P. Durbin and C. Speziale, "Local anisotropy in strained turbulence at high Reynolds numbers," J. Fluids Eng. **113**, 707 (1991).
[3] R. A. Antonia, J. Kim, and L. W. B. Browne, "Some characteristics of small-scale turbulence in a turbulent duct flow," J. Fluid Mech. **233**, 369 (1991).
[4] W. K. George and H. J. Hussein, "Locally axisymmetric turbulence," J. Fluid Mech. **233**, 1 (1991).
[5] X. Shen and Z. Warhaft, "The anisotropy of the small scale structure in high Reynolds number ($R_\lambda \sim 1000$) turbulent shear flow," Phys. Fluids **12**, 2976 (2000).
[6] S. Garg and Z. Warhaft, "On the small scale structure of simple shear flow," Phys. Fluids **10**, 662 (1998).
[7] A. Pumir, "Turbulence in homogeneous shear flows," Phys. Fluids **8**, 3112 (1996).
[8] L. Biferale and I. Procaccia, "Anisotropy in turbulent flows and in turbulent transport," Phys. Rep. **414**, 43 (2005).
[9] I. Arad, B. Dhruva, S. Kurien, V. S. L'vov, I. Procaccia, and K. R. Sreenivasan, "Extraction of anisotropic contributions in turbulent flows," Phys. Rev. Lett. **81**, 5330 (1998).
[10] I. Arad, V. L'vov, and I. Procaccia, "Correlation functions in isotropic and anisotropic turbulence: The role of the symmetry group," Phys. Rev. E **59**, 6753 (1999).
[11] S. Kurien and K. R. Sreenivasan, "Anisotropic scaling contributions to high-order structure functions in high-Reynolds-number turbulence," Phys. Rev. E **62**, 2206 (2000).
[12] S. Kurien, V. L'vov, I. Procaccia, and K. Sreenivasan, "Scaling structure of the velocity statistics in atmospheric boundary layers," Phys. Rev. E **61**, 407 (2000).
[13] L. Biferale and F. Toschi, "Anisotropies in homogeneous turbulence: Hierarchy of scaling exponents and intermittency of the anisotropic sectors," Phys. Rev. Lett. **86**, 4831 (2001).
[14] L. Biferale, D. Lohse, I. M. Mazzitelli, and F. Toschi, "Probing structures in channel flow through SO(3) and SO(2) decomposition," J. Fluid Mech. **452**, 39 (2002).
[15] L. Biferale, I. Daumont, A. Lanotte, and F. Toschi, "Anomalous and dimensional scaling in anisotropic turbulence," Phys. Rev. E **66**, 056306 (2002).
[16] Z. Warhaft and X. Shen, "On the higher order mixed structure functions in laboratory shear flow," Phys. Fluids **14**, 2432 (2002).
[17] A. Staicu, B. Vorselaars, and W. Van de Water, "Turbulence anisotropy and the SO(3) description," Phys. Rev. E **68**, 046303 (2003).
[18] B. Jacob, C. M. Casciola, G. Iuso, and L. Biferale, "Anisotropic fluctuations in turbulent shear flows," Phys. Fluids **16**, 4135 (2004).
[19] C. M. Casciola, P. Gualtieri, B. Jacob, and R. Piva, "The residual anisotropy at small scales in high shear turbulence," Phys. Fluids **19**, 101704 (2007).
[20] C. M. Casciola, P. Gualtieri, B. Jacob, and R. Piva, "Scaling properties in the production range of shear dominated fows," Phys. Rev. Lett. **95**, 024503 (2005).
[21] J. L. Lumley, "Interpretation of time spectra measured in high-intensity shear flows," Phys. Fluids **8**, 1056 (1965).
[22] J. M. Österlund, "Experimental studies of zero pressure-gradient turbulent boundary-layer flow," Ph.D. thesis, KTH, 1999.
[23] J. M. Österlund, A. V. Johansson, H. M. Nagib, and M. H. Hites, "A note on the overlap region in turbulent boundary layers," Phys. Fluids **12**, 1 (2000).
[24] S. V. Saddoughi and S. G. Veeravalli, "Local isotropy in turbulent boundary layer at high Reynolds number," J. Fluid Mech. **268**, 333 (1994).
[25] N. Marati, C. M. Casciola, and R. Piva,"Energy cascade and spatial fluxes in wall turbulence," J. Fluid Mech. **521**, 191 (2005).